JOURNAL OF COMPUTATIONAL PHYSICS 115, 43–55 (1994)

Open Boundary Conditions in the Simulation of Subsonic Turbulent Shear Flows

FERNANDO F. GRINSTEIN

Laboratory for Computational Physics and Fluid Dynamics, Code 6410, Naval Research Laboratory, Washington, DC 20375-5344

Received September 4, 1992; revised November 23, 1993.

Dealing with open boundaries in the computer simulation of unsteady subsonic shear flows presents challenging problems. In practice, only a portion of the flow can be investigated and we must ensure that the presence of artificial boundaries does not pollute the solution in a significant way. One difficulty is related to the basic solution of the physical flow equations and involves choosing appropriate nonlocal open boundary conditions at the outflow boundaries which will adequately bound the computational domain while providing information about the virtual flow behavior outside. A second difficulty is related to the discretized computational problem, for which additional numerical boundary conditions that are consistent with the unsteady flow equations at the boundaries are required for closure. Recent approaches based on characteristic analysis and their practical implementation are discussed. Specific examples are used to illustrate the implementation of state-of-the-art approaches to open boundary conditions and, in particular, the potential sensitivity of subsonic free shear flows to the actual choice of open boundary conditions. This sensitivity is an intrinsic feature of the flows being studied rather than an artifact of the computations. *Ideal* free shear flows do not exist; actual flow realizations are defined by the numerical or laboratory boundary conditions in the experiments.

1. INTRODUCTION

Shear flows such as are present in mixing layers, wakes, and jets (Fig. 1) are of great interest because of their crucial roles in many practical applications. Experimental investigations in idealized geometries have shown that large-scale coherent structures (CS) in these flows dominate the entrainment and mixing processes [1]. The study of the physical properties of CS requires accurate flow data to identify and characterize their main features in order to develop conceptual models and analytic frameworks for their description. Computer simulations and laboratory experiments offer two complementary approaches in this research.

The CS in free (unconfined) shear flows are spatially evolving, and imposing realistic open boundary conditions for their computer simulation is a difficult problem. Because of this, it has frequently been preferred to focus on temporally (as opposed to spatially) evolving calculations using well-posed periodic boundary conditions (e.g., Ref. [2]). This approach can be though of as describing the time evolution of the flow in compact regions. However, major aspects of the growth and dynamics of laboratory turbulent shear-flows, e.g., asymmetric entrainment [3] and feedback phenomena [4], cannot be captured by spatially periodic simulations, since they are intimately associated with the flow development in both space and time. In practice, as in the laboratory investigations, the finite dimensions of the flow domain investigated are unavoidable, and one must determine ways of ensuring that the flow in the regions of interest is not significantly affected by the presence of artificial boundaries. At these open boundaries, the flow of information in both directions must be allowed, non-physical reflections are to be avoided, and the flow must be capable of relaxing in prescribed ways to ambient conditions.

The simulation of subsonic shear flows is based on the numerical solution of the Navier–Stokes (NS) equations with appropriate boundary conditions (BC). This involves dealing with the system of time-dependent, compressible, conservation equations for total mass and energy density and momentum

$$\frac{\partial \rho}{\partial t} + \nabla \cdot \rho \mathbf{V} = 0, \tag{1}$$

$$\frac{\partial (\rho \mathbf{V})}{\partial t} + \nabla \cdot (\rho \mathbf{V}\mathbf{V} + P\mathbf{I} - \Gamma) = 0, \tag{2}$$

$$\frac{\partial E}{\partial t} + \nabla \cdot [(E+P)\mathbf{I} - \Gamma]\,\mathbf{V} + \nabla \cdot (\mathcal{Q}) = 0, \tag{3}$$

where ρ is the mass-density, $\mathbf{V} = (u_1, u_2, u_3)$ is the flow velocity, $\mathbf{I}$ and Γ are the non-dimensional-unit and viscous-stress tensors, respectively, and P is the static pressure. The heat flux $\mathcal{Q}$ is given by

$$\mathcal{Q} = -\kappa \nabla T, \tag{4}$$

where T is the temperature, κ is the thermal conductivity, and γ is the ratio of specific heats. For simplicity we restrict

581/115/1-4

0021-9991/94 $6.00

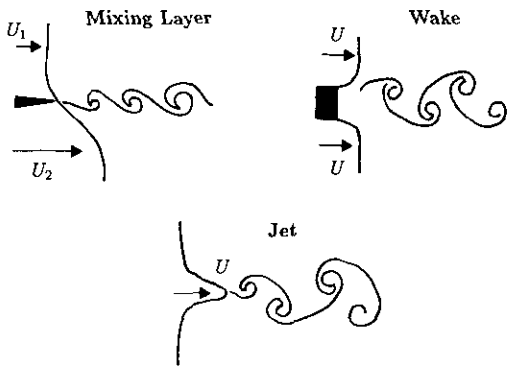

FIG. 1. Basic free shear-flow configurations.

ourselves to ideal gases, in which case the total energy density can be related to the other flow variables by

$$E = \frac{P}{(\gamma - 1)} + \frac{1}{2}\rho \mathbf{V}^2. \tag{5}$$

The number of inflow/outflow open boundary conditions (IOBC), that are required to ensure well posedness and thus completely determine the flow solution in a given finite domain, are well known from theoretical analysis for both Euler and NS equations (e.g., Refs. [5, 6]) and are listed for reference in Table I.

Because of discretization, derivatives can only be approximated at the boundaries, and in order to ensure the closure of the discretized system of equations, additional numerical boundary conditions need to be specified (hereafter referred to as CNBC). The standard procedure is to introduce these new conditions by defining the behavior of physical variables at an extra row of *guard cells* surrounding the domain. The CNBC are to be clearly distinguished from the discretized representations of IOBC (hereafter also denoted by IOBC), which are required in order to uniquely define the solution of the non-discretized fluid-dynamical problem.

As a practical example, consider the 3D Euler equations and the problem of specifying the necessary open boundary conditions in the x_1-direction, which we assume to be the streamwise direction. At the inflow boundary, the needed four IOBC can be chosen to be the specified free-stream values of mass-density and velocities, ρ, u_1, u_2, u_3, and an additional CNBC for the closure of the discretized system of equations is needed to relate the guard-cell values of the static-pressure—or equivalently, of the total energy—to information on the flow inside of the domain (Section 4). If only the pressure gradient is specified at the inflow boundary, the pressure itself should be specified elsewhere at the boundaries to prevent the possible drift of its value. However, *specifying* the pressure (or any of the other primitive flow variables) at the downstream outflow boundary of a finite-sized computational domain will *define* flows which might be physically valid but do not correspond in general to spatially developing shear flows of interest. We need to specify both the pressure at $x_1 = \infty$ and the *way* in which the pressure at the boundary physically relaxes to the ambient value P_∞. Because the transition of the flow to ambient conditions is in general a function of the flow features inside the computational domain—beyond those strictly in the neighborhood of the outflow boundary—these flows require the specification of nonlocal outflow BC. In addition, CNBC are needed to completely determine the gradients of ρ, u_1, u_2, u_3, at the outflow boundary. At open boundaries in the shear-flow cross-stream directions x_2 and x_3, special considerations are needed to define BC, since the flow does not have a specific inflow or outflow behavior there and transparency to acoustical propagation must be ensured. Although much of the formalism on open BC that is discussed below in Section 3 is also appropriate for the cross-stream boundaries, the treatment of these boundaries is not specifically addressed in this paper, where the focus is on streamwise inflow and outflow BC.

In the present paper, we address two basic practical difficulties in uniquely determining a numerical free shear-flow solution. One is related to the basic solution of the physical flow equations and involves choosing appropriate nonlocal IOBC at the downstream outflow boundary. The second difficulty is related to the discretized (computational) problem and involves ensuring that the CNBC required for closure are prescribed in a consistent way. In Section 2 we discuss the limitations of traditional simplified approaches to dealing with open boundaries based on using time-independent boundary conditions. Recent improved approaches are reviewed in Section 3, and their practical implementation for actual subsonic (compressible) shear flows is discussed in Section 4. Final remarks are presented in Section 5.

TABLE I

Number of IOBC Required for Well-Posed 3D Subsonic Flow

	Number of IOBC	
Type	Euler	NS
Inflow	4	5
Outflow	1	4

2. TIME-INDEPENDENT APPROACHES

In these approaches to defining BC one relies much more on the effective presence of buffer regions surrounding the flow region of interest than on relating self-consistently the shear-flow solution to actual boundary conditions. It basically involves using some sort of "reasonable" time-inde-

pendent outflow BC—usually chosen based on simplicity considerations—which are imposed as "far away as possible.." In that respect, this approach is very similar to that used in the laboratory to choose the actual size of the experimental facilities and the nature of their boundaries so that they will affect the flow studied as little as possible. Besides effectively separating the flow-regions of interest from the physical location of the boundaries, the buffer regions can also be effectively used as "viscous-sponges" by damping and/or absorbing to some extent spurious acoustic disturbances that may be generated at the open boundaries. In practice, this can be implemented by introducing strong numerical dissipation in the buffer regions, e.g., by stretching the size of the computational cells, or by actually adding appropriate artificial dissipation terms to the flow equations.

Practical computer simulations using such time-independent approaches have been reported in the literature for various flow configurations and regimes. Typical outflow BC use time-independent extrapolations of the flow variables at the boundaries [7–11], which at times are also used in conjunction with either finite-to-infinite mappings [7], or stretched grids and pressure extrapolations to approach ambient conditions [8]. In the case of the incompressible calculations of Ref. [7], for example, the emphasis of the study was on unsteady flow features, and minimizing the effect of the outflow boundary conditions on the flow solution was approached by organizing the flow using forcing at the inflow and restricting the time-dependent study to relatively short times. In the calculations of Ref. [8] a temporal statistical study of a compressible (subsonic) unforced jet was involved, in which relatively large stretched-grid buffer-regions were used to ensure stable statistical results in the initial jet region. In Refs. [9–11] computer simulations of incompressible reactive mixing layers [9] and plane wakes [10, 11] used homogeneous Neumann outflow conditions based on either first [10] or second-order [9, 11] velocity derivatives on domains with finite streamwise extent.

In general, the use of *viscous-sponge* buffer regions and/or simplified time-independent outflow BC is not necessarily consistent with the flow equations and/or physical intrinsic feedback effects present in actual physical realizations of free shear flows. As a consequence, the usefulness of this approach is restricted to isolating a region of the flow for relatively short-timed unsteady simulations, or for simulations that are either forced or mainly focused on the initial shear-flow dynamics. Otherwise, the approach may be expensive or inadequate for unforced calculations and/or if very long runs are required for stable temporal statistics.

Considerations of computational efficiency and accuracy make it desirable to eliminate the use of buffer regions and focus more on the actual choice of boundary conditions and in particular, on the adequacy of specific CNBC for the shear-flow problem posed. A certain amount of "artistic work" is traditionally involved in choosing CNBC. Although there is no general guideline for the choice of CNBC, one can show that relatively simple and apparently reasonable, time-independent outflow CNBC can lead to unphysical and, eventually, unstable solution behaviors. In order to see this, consider a model equation for mass-transport in the direction (x_1) across a boundary, obtained by linearizing the continuity equation and reducing it to an advection equation,

$$\partial\rho/\partial t + u_1 \partial\rho/\partial x_1 = 0, \tag{6}$$

where $u_1 \geqslant 0$ is the local x_1-component of the outflow velocity near the boundary. We discretize this equation by a first-order upwind scheme and relate the outflow-guard-cell value ρ_G^n at the nth integration cycle as a function of ρ_G^{n-1} and the Nth cell value at the boundary, ρ_N^{n-1}, from the previous integration cycle by the expression

$$\rho_G^n = \rho_G^{n-1}(1-\alpha) + \alpha\rho_N^{n-1}, \tag{7}$$

where

$$\alpha = u_1\,\Delta t/\Delta x_{\text{out}} = c(\Delta x_{\min}/\Delta x_{\text{out}})\,u_1/(u_1+a)_{\text{peak}}, \tag{8}$$

Δt is the integration timestep, c and $a = (\gamma P/\rho)^{1/2}$ are the Courant number and sound speed, and $\Delta x_{\min}$ and Δx_{out} are the minimum spacing in the grid and the spacing at the outflow boundary, respectively. Using (7) we can assess the quality of frequently used lower-order outflow CNBC defining guard-cell values at the current integration cycle using zeroth order extrapolations from the boundary values,

$$\rho_G^n = \rho_N^{n-1}, \tag{9}$$

which corresponds to choosing $\alpha = 1$ in (7). For subsonic flows (say, Mach numbers $M < 0.5$) and Courant numbers $c < 0.5$, from (8) we have $\alpha < 0.17$, which indicates that the effect of the time derivative cannot be neglected and a zeroth order extrapolation to define the guard-cell values at an outflow boundary is inconsistent with the flow equation (6) and unrealistic for these flow regimes. In particular, (8) indicates that the approximation is worse for smaller local values of the Mach number, i.e., on the slower side of the simulated shear flow. In the incompressible regime, it has been shown that spurious reflections at the boundaries generated by the use of inadequate CNBC can induce artificial self-sustained global instabilities in free shear flows [12].

3. RECENT IMPROVED APPROACHES

From the purely mathematical point of view, so-called *non-reflective* boundary conditions of various types have been proposed for hyperbolic equations, as recently reviewed by Givoli [13]. The general idea is to use knowledge on the mathematical solution outside of the computational domain to define conditions which will minimize spurious reflections at the artificial boundaries. These *non-reflective* conditions are generally non-local and can be either totally absorbing (as in, e.g., Ref. [14]) or allow for some *natural reflections* to occur (e.g., Ref. [15]). Such natural reflections should be built in the outflow IOBC in the simulation of subsonic free shear-flows if we are to have emulation of feedback effects, by which events that are assumed to virtually occur outside of the computational domain can effectively influence the flow inside.

Although it may appear obvious, it is generally overlooked that choosing "appropriate" IOBC in numerical shear-flow studies emulating laboratory realizations is only meaningful to the extent that the corresponding outflow (and other) BC in the shear-flows to be simulated are well specified. Otherwise, the choice of IOBC is subjective, since it amounts to guessing the nature of the BC involved in the "well-established" experimental results in the literature—where only information on the initial (inflow) BC is typically reported. In the laboratory experiments, the effects of boundary conditions other than initial conditions has been regarded (if at all) as due to "unavoidable facility-dependent background disturbances," which are suggested to be responsible for observed differences between experimental results [16]. In fact, inspection of Table I clearly indicates that specifying the inflow boundary conditions is not sufficient to completely specify the flow inside a prescribed finite-sized open domain. Thus, these "background disturbances" in the experiments actually correspond to the specifically distinct facility-enforced BC. The issue is further addressed from the laboratory-experimentalist's point of view by George [17]:

> Unlike the theoretician, the experimentalist already knows the solution, for it is the flow he has realized. His objective is to find which equations and which boundary and initial conditions his solution corresponds to, and then to compare them and his results to those dealt with by the theoretician.

An implicit assumption in the laboratory and numerical studies is that the flow-solution associated with the combined experimental-domain/BC system approximates either a limiting ideal regime in which the free shear flow becomes independent of the downstream BC, or for which the solution is nearly the same as that in an unbounded domain. However, since *both* initial *and* other boundary conditions have a role in specifying the flow-solution and feedback effects are unavoidable for subsonic flows, the existence of such an ideal regime that is independent of BC is unrealistic. Moreover, since the traditionally expected universality of asymptotic self-similar behaviors is now in doubt [18], even in the limiting case of idealized (unbounded) free shear-flows, the specification of the outflow IOBC is probably not unique.

Focusing now on the problem of specifying the CNBC needed for closure of the discretized system of equations, a basic guideline should be to require that the CNBC be consistent with the IOBC prescribed for the non-discretized problem and approximate the unsteady flow equations as accurately as possible at the boundaries. For hyperbolic equations, for example, it is well known that the nth order internal solution of the equations requires at least $(n-1)$th order additional CNBC to preserve the formal spatial accuracy of the calculations [19]. The goal is to ensure that the expected flow behavior outside the computational domain is properly and *consistently* imposed on the solution inside, a requirement that is frequently overlooked. The consistency requirement demands that in the continuum limit such CNBC be compatible with the flow equations and IOBC and do not generate distinctly new BC overspecifying the fluid dynamical problem. However, this guideline is not sufficient to uniquely determine the CNBC and some degree of ambiguity appears to be unavoidable, unless additional requirements are imposed.

Beyond the issue of specifying IOBC and CNBC for the particular shear flow of interest, we need to deal with the problem of imposing them in the practical simulations. For hyperbolic equations, an adequate framework has been proposed by Thompson [14, 20] that is based on a characteristic-analysis formalism for the Euler equations. The problem of imposing the BC is addressed by focusing on the terms of the flow equations containing derivatives with respect to the (local) direction perpendicular to the inflow/outflow boundary. These terms require special numerical treatment because they partially depend on incoming information from outside of the computational domain. Other terms in the flow equations, not containing these derivatives, can be treated in the neighborhood of the boundary in the same way as inside the computational domain. For the sake of the discussion, let x_1 be the *local* inflow/outflow direction. Then, these derivative-terms can be conveniently cast in terms of the amplitude-variations of characteristic waves $\{\mathscr{L}_i\}$ [20],

$$\frac{\partial(\rho u_1)}{\partial x_1} = \frac{1}{a^2}\left[\mathscr{L}_2 + \frac{1}{2}(\mathscr{L}_1 + \mathscr{L}_5)\right], \tag{10}$$

$$\frac{\partial(a^2 \rho u_1)}{\partial x_1} = \frac{1}{2}(\mathscr{L}_1 + \mathscr{L}_5), \tag{11}$$

$$u_1 \frac{\partial(u_1)}{\partial x_1} = \frac{1}{2\rho a}(\mathscr{L}_5 - \mathscr{L}_1), \tag{12}$$

$$u_1 \frac{\partial(u_2)}{\partial x_1} = \mathscr{L}_3, \tag{13}$$

$$u_1 \frac{\partial(u_3)}{\partial x_1} = \mathscr{L}_4, \tag{14}$$

where the amplitudes $\mathscr{L}_i$ are defined by

$$\mathscr{L}_1 = \lambda_1 \left(\frac{\partial P}{\partial x_1} - \rho a \frac{\partial u_1}{\partial x_1} \right), \tag{15}$$

$$\mathscr{L}_2 = \lambda_2 \left(a^2 \frac{\partial \rho}{\partial x_1} - \frac{\partial P}{\partial x_1} \right), \tag{16}$$

$$\mathscr{L}_3 = \lambda_3 \frac{\partial u_2}{\partial x_1}, \tag{17}$$

$$\mathscr{L}_4 = \lambda_4 \frac{\partial u_3}{\partial x_1}, \tag{18}$$

$$\mathscr{L}_5 = \lambda_5 \left(\frac{\partial P}{\partial x_1} + \rho a \frac{\partial u_1}{\partial x_1} \right), \tag{19}$$

and the $\{\lambda_i\}$ are the characteristic velocities

$$\lambda_1 = u_1 - a, \tag{20}$$

$$\lambda_2 = \lambda_3 = \lambda_4 = u_1, \tag{21}$$

$$\lambda_5 = u_1 + a. \tag{22}$$

The characteristic velocities λ_1 and λ_5 represent the velocity of sound waves moving in the $-x_1$ and $+x_1$ directions, respectively, while λ_2, λ_3, and λ_4 are the advection velocities for entropy, u_2 and u_3, in the $+x_1$ direction.

In the formalism by Thompson [20] the problem of determining the derivatives at the boundaries in (10)–(14) is reduced to that of locally evaluating the amplitudes $\mathscr{L}_i$, where those associated with outgoing waves are determined using CNBC generated with one-sided finite-difference expressions based on information from the inside of the computational domain. The problem is to determine the amplitudes associated with the incoming waves, which involve information that must be externally specified. This information can be provided by the IOBC, when these are given in terms of the $\mathscr{L}_i$ as in, e.g., Ref. [20]. In the more general case, however, the information on the incoming waves is not readily available. Poinsot and Lele [21] propose specifying the $\mathscr{L}_i$ for incoming waves, based on the *local* one-dimensional inviscid (LODI) equations in the direction perpendicular to the boundary (Appendix) for which the amplitudes $\mathscr{L}_i$ can be determined exactly using the IOBC for the problem under consideration. Although this approach is limited by the extent to which the one-dimensional characteristic analysis is appropriate for the problem under consideration, it provides a systematic and consistent way of prescribing the $\mathscr{L}_i$.

In many cases, the nature of the shear-flow dynamics at the *open* boundaries is essentially inviscid; viscous effects can be neglected there and it suffices in practice to use the derived inviscid CNBC for the NS equations. This is assumed to be the case in the present paper. Otherwise, the CNBC derived with this approach need to be supplemented with appropriate additional (viscous) conditions. In the next section, we discuss relevant issues that are involved in the practical specification and implementation of IOBC and CNBC in the framework of Refs. [20, 21]. The test cases examined below illustrate the potential sensitivity of the dynamics of a subsonic shear flow to the actual choice of IOBC and CNBC.

4. EXAMPLES OF BOUNDARY CONDITIONS FOR SHEAR FLOWS

The exact nature of feedback effects in subsonic shear flows is problem dependent in general. In particular, feedback effects due to coupling between inflow and outflow IOBC are expected on physical grounds for subsonic shear flows and are certainly unavoidable. In this section we focus on two problems which, by construction, allow us to isolate to some extent the effects of streamwise inflow and outflow BC: (1) the initial development of the KH instability in an unforced mixing layer; and (2) the dynamics of a developed single-frequency forced mixing layer. To simplify the discussion, two-dimensional cases are studied here, in which (i) viscous effects are neglected; (ii) rectangular computational domains are used where the relevant inflow and outflow directions are fixed and coincident with the streamwise direction and for which the boundaries in the cross-stream direction are chosen far away from the shear-flow regions. The cross-stream boundaries are approached on both sides with a geometrically stretched grid, while the grid is uniform in the streamwise direction and evenly spaced within the flow-region of interest. Addressing the improved formulation of BC at the side boundaries, the definition of generalized IOBC and CNBC in order to deal with viscous effects, as well as the treatment of corners and (3D) edges in the boundaries, is beyond the scope of the present paper. Appropriate extensions of the formalism can be pursued with this regard following the approaches proposed in Refs. [20, 21].

In following the *one-dimensional* framework of Refs. [20, 21] for dealing with inflow/outflow boundaries, one should note that assumptions are made: (1) that we can focus on a "characteristic flow direction" normal to the boundary, not necessarily coincident with the *actual* local characteristic direction of the unsteady flow in general; (2) that the local fluid velocity normal to the boundary does not vanish and has a well-defined sign, so that a well-defined number of characteristic incoming waves (and thus of

IOBC) are involved at the corresponding boundary. These assumptions are quite reasonable in some cases, such as, at an inflow boundary normal to an initially laminar parallel shear shear flow. However, as shown below, depending on how far the flow features near the outflow boundary are from being one-dimensional, assumption (1) may be less appropriate and more general multidimensional approaches may be required.

Inflow Conditions for the Unforced Mixing Layer

In the general three-dimensional case, there is one outgoing wave at the inflow boundary (associated with $\mathscr{L}_1$) and the other four amplitudes are associated with incoming waves which must be determined using IOBC, e.g., specifying ρ, u_1, u_2, u_3. We need to give a fifth condition (CNBC) to determine, e.g., $\partial P/\partial x_1$.

Since we are fixing u_1 at the inflow, $\partial u_1/\partial t = 0$ holds there, and when used with (A.3) from the Appendix, it follows that

$$\mathscr{L}_5 = \mathscr{L}_1. \tag{23}$$

Using (23) in (A.2) yields

$$\frac{\partial P}{\partial t} + \mathscr{L}_1 = 0, \tag{24}$$

where, since $\mathscr{L}_1$ is associated with an ougoing wave at the inflow boundary, it may be evaluated at the guard-cells using (15) and one-sided differences based on information inside the computational domain, to calculate the guard-cell pressures, P_G^n, at the current integration time in terms of those at the previous cycles. A low-order approximation to P_G^n can be obtained using (15) in (24) in the form

$$P_G^n = P_1^{n-1} + (P_G^{n-1} - P_1^{n-1})(1 + \varepsilon_G^{n-1}) + \varepsilon_G^{n-1}\rho_o a_G^{n-1} \times [(u_1)_1^{n-1} - (u_1)_o] + \mathscr{O}(\Delta t\, \Delta x_1), \tag{25}$$

where indices "j" and "k" are assumed and omitted corresponding to directions "2" and "3", respectively, the lower index "o" refers to the specified initial (free-stream) inflow conditions, and $\varepsilon_G^{n-1} = \Delta t((u_1)_o - a_G^{n-1})/\Delta x_1$.

A simpler, lower-order form of (25),

$$P_G^n = P_1^{n-1}, \tag{26}$$

differing from (25) in terms of order $\mathscr{O}((\Delta t)^o\, \Delta x_1)$, has been extensively used in free shear-flow simulations (e.g., Refs. [4, 8]) and loosely regarded as a *zero-gradient* condition on the pressure. It should be noted, however, that in these simulations the Courant number is fixed, so that Δt and Δx_1 are linearly related, and upon replacing $P_1^{n-1} = P_1^n + \mathscr{O}(\Delta t)$ in (26), we (formally) obtain

$$P_G^n = P_1^n + \mathscr{O}(\Delta x_1), \tag{27}$$

which is *not* a finite-difference representation of $\partial P/\partial x = 0$. Such a zero-pressure-gradient CNBC is inconsistent with the flow equations and would thus be inadequate.

Figure 2 shows the two-dimensional flow configuration considered in Ref. [4], in numerical simulations of compressible, spatially evolving, unforced, planar shear flows used to investigate the role of feedback in the reinitiation of vortex roll-up. The focus of this work was on the development of the instabilities due to the presence of an inflectional velocity profile, during a time interval that is short enough to ensure that it is not influenced by events at the outflow boundary. Because of the way in which this problem was set up, it is ideally suited to isolate and assess the effects of CNBC at the inflow.

Two coflowing laminar air streams enter a long chamber defined by two walls. The mixing layer is initialized uniformly at STP everywhere. For the specific examples discussed here, the mean Mach number is, $M = \bar{U}/a = 0.3$ and the free-stream velocities are, $U_1 = 2 \times 10^3$ cm/s and $U_2 = 2 \times 10^4$ cm/s, where $\bar{U} = (U_1 + U_2)/2$ is the mean free-stream velocity. The initial and inflow velocity profiles are defined in terms of the hyperbolic tangent profile $U(y) = \bar{U}[1 + R \tanh(y/2\theta_o)]$, where $R = (U_2 - U_1)/2\bar{U}$, which approximates quite well the profiles in the initial region of the experimental shear layers. The instability mechanism of these inflectional velocity profiles is inviscid and viscous diffusion only damps the process. It is then adequate to investigate the dynamics of the instabilities based on the solution of the inviscid, time-dependent, compressible conservation equations for ideal gases.

In the case-studies examined here, the equations are solved using a nonlinear, explicit, compressible, finite-difference flux-corrected transport (FCT) algorithm [23]. The accuracy of the particular version of the FCT algorithm used in these simulations is fourth order in phase and second order in amplitude and time, and the simulations were performed for fixed Courant number (0.5). Thus, the conditions imposed at the boundaries must be at least first-order accurate in space and time to preserve the formal global accuracy of the flow solution [20]. Inflow and outflow boundary conditions were imposed in the streamwise direction. Reflecting free-slip wall conditions were imposed in the cross-stream direction.

The inflow IOBC used in the two-dimensional studies of Ref. [4] specify the density and velocities and impose

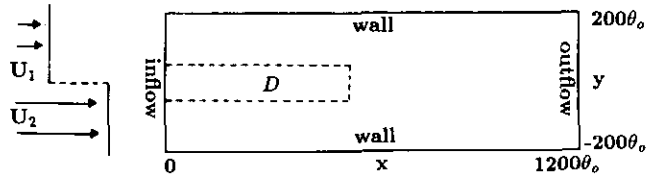

FIG. 2. Flow configuration for the unforced mixing layer.

CNBC on the energy. These conditions were implemented by setting the guard-cell values for the mass and velocity densities at the inflow equal to their specified free-stream values:

$$\rho_G = \rho_o, \tag{28a}$$

$$(u_1)_G = (u_1)_o = U(y), \tag{28b}$$

$$(u_2)_G = 0, \tag{28c}$$

and using (26) for the pressure. The guard-cell values of the energy were calculated through the equation of state as a function of the corresponding values of mass density, momenta, and pressure. At the outflow, linear advection equations were imposed using the local velocity near the boundary, and the pressure was relaxed towards a specified ambient value. As stated above, however, the test cases discussed below were carried out (by design) during times sufficiently short so that the exact nature of the boundary conditions specified at the downstream boundary would have no effect on the flow features investigated.

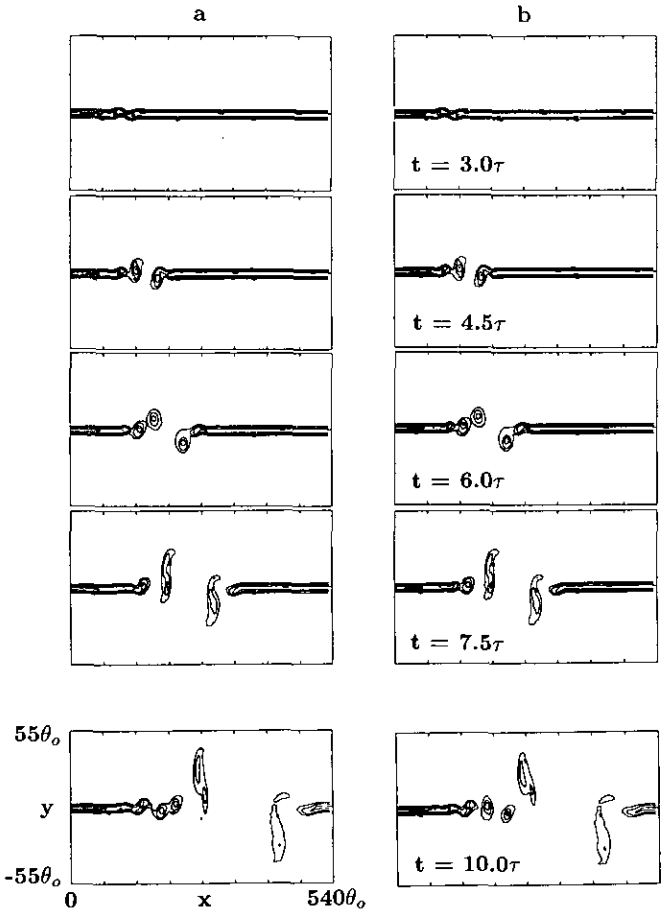

FIG. 3. Initial development of the unforced mixing layer in terms of vorticity contours. The regions shown in the figures correspond to the subregion denoted by D in Fig. 2. CNBC used at the inflow: (a) Eq. (25); (b) Eq. (26).

The small velocity perturbation triggering the KH instability appears early in the shear layer near the inflow boundary and is caused by an initial mismatch due to discretization between the initial conditions and the inflow boundary conditions (see also Ref. [12]). The perturbation is impulsive (broad-band) and of peak level less than 0.2% $\bar{U}$. Figures 3a and 3b compare the initial development of the instabilities for $R = 0.82$ and $M = 0.3$, using (25) and (26), respectively, in terms of sequences of vorticity contours, in order to examine the sensitivity of the shear flow to changes in the CNBC at the inflow. Specifically, we are interested in assessing the dependence on CNBC of the *receptivity* of the initial shear layer to acoustic disturbances originated by the vortex dynamics downstream.

As the initial instability grows and is convected downstream, the thin initial vorticity distribution along the centerline is distorted, becomes concentrated locally in two regions, and then breaks and forms a pair of vortices. The frames at time $t = 4.5\tau$ show the reinitiation of the instabilities on both sides of the initial vortex pair. At later times, the vorticity layer breaks up further, and new vortices—better defined on the left of the vortex-pair—roll up, roll around, and merge with the older neighboring vortices. This is followed by subsequent roll-ups and further mergings involving the original successively enlarged vortices.

The area shown in the frames in Fig. 3 corresponds to the small region D in Fig. 2. By construction, the times of the frames in Fig. 3 are early enough to ensure that any spurious reflections of acoustic signals at the outflow boundary have not had enough time to affect the flow or even to occur. Moreover, the observed pattern of global self-sustaining instabilities, in which new vortex-roll-ups are triggered in the initial shear layer by pressure disturbances originating in the fluid accelerations downstream, is also independent of the presence of the walls [4].

As in the laboratory experiments, the inflow conditions in the simulation actually *define* the behavior of the initial shear layer and its receptivity properties. The initial conditions for this problem were defined by a specified inflow flux that was provided by fixed mass density, an inflectional streamwise velocity profile, and a zero-cross-stream velocity. The conditions used here impose a floating condition on the pressure at the inflow through (25) or (26). This allows finite (unsteady) cross-stream pressure differences to appear in the initial shear layer in response to acoustic waves and potential pressure fluctuations generated by events downstream, thus allowing (physical) feedback to occur. Comparison of the corresponding frames in Figs. 3a and 3b, including the first seven vortex roll-up events shows that the basic pattern of self-sustained vortex roll-up with mean characteristic time τ is independent of whether (25) or (26) are used at the inflow. On the other hand, the differences between the bottom frames of Figs. 3a and 3b indicate

that the details and phase reference of the subharmonic feedback loop [2] connecting the vortex pairing at $t \sim 6\tau - 7\tau$, with the early stages of a new merging suggested in the bottom frames of Fig. 3, are clearly sensitive to the accuracy of the CNBC used at the inflow. For the accuracy of the numerical scheme used here, the use of (25) as CNBC should be preferred for studies requiring accurate determination of vortex-merging locations in space and time.

Outflow Conditions for the Forced Mixing Layer

The dynamics of a single-frequency forced mixing layer are essentially characterized by vortices rolling up at the forcing frequency. The initial shear layer is modulated by pressure fluctuations that originated with the fluid accelerations downstream within the computational domain and by those virtually occurring outside—effectively emulated by the incoming information imposed by the outflow IOBC. As shown below, depending on the flow history and on the nature of these feedback effects, vortex mergings may also occur. In what follows, we illustrate the sensitivity of the flow dynamics to the choice of IOBC at the outflow.

At an outflow boundary of a subsonic 3D flow configuration, there are four outgoing waves and one incoming wave (associated with $\mathscr{L}_1$) for which we need to specify an IOBC. Poinset and Lele [21] propose specifying the amplitude $\mathscr{L}_1$ in the form

$$\mathscr{L}_1 = (u_1 - a)\left(\frac{\partial P}{\partial x_1} - \rho a \frac{\partial u_1}{\partial x_1}\right) = \mathscr{K}(P - P_\infty) + \mathscr{L}_1^{\text{exact}}, \tag{29}$$

with $\mathscr{K} = \sigma(1 - \mathscr{M}^2)\, a/L$, as defined by Rudy and Strikwerda [22], where $\mathscr{M}$ is the maximum free-stream Mach number in the flow, a is the local sound speed at the outflow boundary, and the characterictic length L and parameter σ have to be specified, and where $\mathscr{L}_1^{\text{exact}}$—to be determined, based on the assymptotic properties of the solution outside of the computational domain—ensures "an accurate matching of the derivatives between both sides of the boundary," while the first term on the right-hand side "keeps the mean pressure values around the reference value P_∞."

For $\sigma = 0$ and $\mathscr{L}_1^{\text{exact}} = 0$ we obtain a so-called *perfectly* non-reflecting condition [21] of the type used in the work by Thompson [20],

$$\frac{\partial P}{\partial x_1} - \rho a \frac{\partial u_1}{\partial x_1} = 0. \tag{30}$$

When more than one spatial dimension is involved, however, condition (30) is only the first (lowest-order) in a hierarchy of approximations to a non-reflecting condition for multidimensional problems derived by Engquist and Majda [24]. Thus, for these more general problems, (30) is not *perfectly* non-reflecting and at best can only be regarded as enforcing relatively-low "reflectivity" at the open boundary—presumably smaller when the flow features are more nearly one-dimensional. As a consequence, when using (29) in the general multidimensional case, incoming waves not controlled by $\mathscr{L}_1^{\text{exact}}$ and $\mathscr{K}$ can also be expected.

In principle, we need five additional CNBC to determine $\partial\rho/\partial x_1$, $\partial\rho u_1/\partial x_1$, $\partial\rho u_2/\partial x_1$, $\partial\rho u_3/\partial x_1$, and $\partial E/\partial x_1$ at the outflow boundary. In practice, however, four independent such conditions suffice, since the guard-cell value for one of the primitive variables such as E can be determined based on the guard-cell values of the others using relations such as (5). The necessary CNBC can be generated from the LODI (A.1)–(A.6), which for a generic primitive flow variable Q typically have the form

$$\frac{\partial Q}{\partial t} + F(\rho, a, M, \mathscr{L}_i) = 0. \tag{31}$$

In the lowest order of approximation, from (31) we obtain

$$Q_G^n = Q_G^{n-1} - \Delta t\, F_G^{n-1} + \mathscr{O}((\Delta t)^2), \tag{32}$$

where the amplitudes $(\mathscr{L}_i)_G^{n-1}$ in F_G^{n-1}, can be evaluated using a given expression such as (29) for $i = 1$, and using (15)–(19), the flow-variable information at the previous cycle, and one-sided differences, for $i > 1$. Conditions actually amounting to approximations to these CNBC have been previously considered [25], using linear advection of Q at the outflow boundary with the local streamwise velocity (also for the basis for defining so-called *force-free* boundary conditions in Ref. [20]).

The basic flow configuration considered in the following tests of outflow IOBC is shown in Fig. 4. It is similar to that in Fig. 2, except for the free-stream boundary conditions (rather than free-slip wall BC) imposed on the side-boundaries. An initial step-function velocity profile is used with $R = 0.5$ and $M = 0.38$. The forcing perturbation added to the inflow transverse velocity was sinusoidal, with (Strouhal) frequency $\text{St} = f\theta_o/\bar{U} = 0.028$, and rms-level $0.02\bar{U}$, where θ_o is the initial vorticity thickness of the mixing layer.

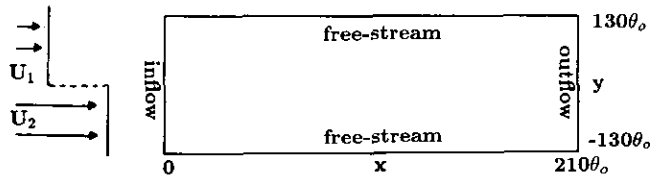

FIG. 4. Flow configuration for the single-frequency forced mixing layer (Runs I–III).

Since examining the effects of the outflow BC on the flow is the main objective of these examples, no streamwise buffer region is used in the simulations and the whole streamwise extent of the computational domain is displayed in Figs. 5–7 below. For these studies, conditions (28) at the inflow, were replaced by

$$\rho_G = \rho_o, \tag{33a}$$

$$(u_1)_G = (u_1)_o = U(y) + A\sin(2\pi f t), \tag{33b}$$

$$(u_2)_G = 0, \tag{33c}$$

and used there in conjunction with the floating pressure condition

$$\begin{aligned} P_G^n = {} & P_1^{n-1} + (P_G^{n-1} - P_1^{n-1})(1+\varepsilon_G^{n-1}) \\ & + \varepsilon_G^{n-1}\rho_o a_G^{n-1}[(u_1)_1^{n-1} - (u_1)_o] \\ & + \rho_o a_G^{n-1}(u_1')^n \Delta t, \end{aligned} \tag{34}$$

which is derived from the LODI (A.2) using (33) and differs from (25) only on the term accounting for the unsteady velocity perturbation, $u_1' = \partial(u_1)_o/\partial t \neq 0$, at the inflow. Because of the forcing at the inflow, the shear-layer development was found to be quite insensitive to changes in the pressure boundary condition there (e.g., virtually identical results were found when using condition (26) instead of (34) at the inflow).

The case studies discussed below involved the same reference ambient pressure P_∞, fixed initial conditions and computational domains, CNBC of the form (32) for ρ, ρu_1, ρu_2, and ρu_3 and (29) as IOBC were used at the outflow, with $\mathscr{L}_1^{\text{exact}} = 0$, $\mathscr{M} = 0.57$, and $L = 130\theta_o$, and varying σ ($\sigma = 0$, 2.7, and 10.8, for Runs I–III, respectively).

Test of these IOBC in conjunction with similarly defined CNBC based on LODI were reported in Ref. [21], including the propagation in a direction normal to the outflow boundary of: (1) a one-dimensional acoustical wave, and (2) a two-dimensional vortex. In test case (1), the one-dimensional nature of (29) is adequate, and spurious reflections—due to numerical discretization—were found to be minimal; in the case of the vortex propagation, where additional reflections can be expected, the residual vorticity left behind after the vortex is convected out of the computational domain was found to be four orders of magnitude smaller than the peak initial vortex magnitude (two orders smaller than when using straight extrapolation CNBC). These results were reproduced in similar tests carried out in the present work to check on the accuracy of the numerical implementation of the BC.

Tests involving the convection of an isolated vortex through an open boundary are important to address the significance of using consistently defined CNBC to ensure smooth vorticity propagation through an outflow boundary, a requirement of great importance in the simulation of turbulent shear flows. With these idealized tests, however, the potential interaction of the residual leftovers in the computational domain with a *receptive* spatially developing mixing layer are not modelled and, thus, the role of upstream feedback effects induced by events at outflow boundaries in a *real* simulation cannot be assessed. The significance of even relatively weak feedback effects can be expected, based on previous simulation of unforced mixing layers [4], where *naturally* induced pressure fluctuations $\partial P/\partial y \times \theta_o/P_\infty \sim 10^{-4}$ were found involved in triggering reinitiation of vortex roll-ups in compressible ($M = 0.3$) mixing layers. These aspects of the implementation of the one-dimensional IOBC/CNBC approach of Ref. [21] for free shear flows are addressed in what follows.

Figure 5 shows the initial flow development in the forced free mixing layer, over a time interval of about seven forcing perids ($\tau = f^{-1}$). The initiation of the instabilities triggered by an impulsive start is similar to that observed in the unforced case (Fig. 3). The figure also indicates the formation of smaller vortical structures upstream of the vortex roll-ups due to feedback, which are immediately engulfed by the latter vortices. Otherwise, vortex mergings tend to be

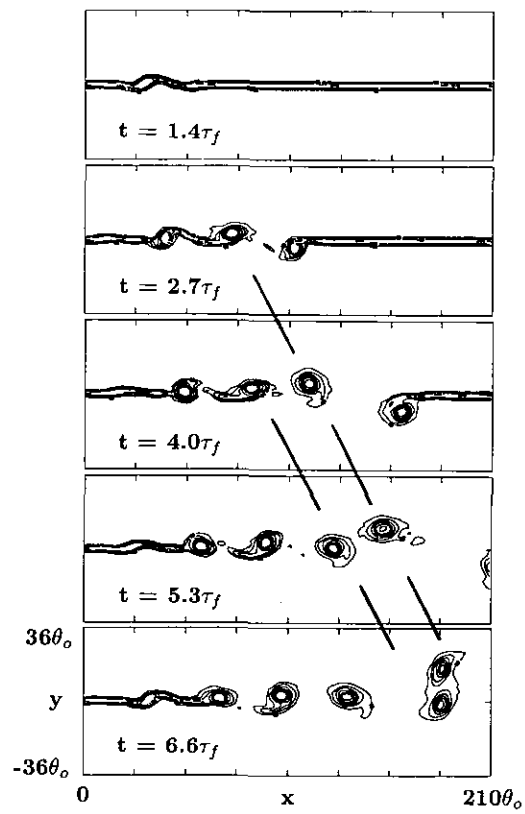

FIG. 5. Initial development of the forced mixing layer in the domain of Fig. 4 in terms of vorticity contours. Left and right boundaries of the frames correspond to the actual inflow/outflow boundaries in the computational domain.

inhibited because of the forcing, and a first merging event between vortices associated with the forcing frequency occurs after about five vortex roll-ups. This initial development of the flow was found to be virtually the same for Runs I–III, and thus independent of the outflow IOBC.

Before examining upstream effects of changing the amount of incoming information allowed by (30) in terms of σ, we need to assess the degree of "transparency" that can be expected from the present one-dimensional IOBC/CNBC approach. Such an assessment can be obtained by considering the "non-reflective" limit ($\sigma = 0$) and examining the effects of changing the relative location of the downstream boundary. The simulated flow of Run I is compared with a separate simulation (Run Ix) carried out under identical conditions on a computational domain with the outflow boundary located farther downstream, with a streamwise extent 50% longer than that in Fig. 4. Restricting this comparison to suitably chosen short times, we can isolate effects of reflections on the downstream boundary in the domain of Fig. 4, using as reference the results in the longer domain for which potential reflections in the downstream boundary have not had the same possibility of affecting the flow.

Comparison of results from Runs I (left column) and Run Ix (right column), are shown in Fig. 6, where the flow visualization for Run Ix is restricted to the portion of the extended domain coinciding with that of Fig. 4. Towards the bottom of the sequence shown in Fig. 5—and the top of the sequence in Fig. 6a—the initial flow transient is being convected out of the computational domain and the flow features near the downstream boundary are far from being one-dimensional as the first vortex pairing event progresses. It is then only natural to expect that some sort of reflections will be allowed at the downstream boundary by the one-dimensional non-reflective IOBC, as the system of pairing vortices convects through the boundary at $t \approx 7\tau$ for Run I (and at $t \approx 10\tau$ for Run Ix). Disturbances acoustically propagating upstream originated by these reflections will add to those generated by the vortex pairing process itself [4]. Through a feedback mechanism, the initial shear layer is disturbed by these subharmonic perturbations generated downstream with a dominant wavelength equal to twice that of the imposed wavelength. Such disturbances, in turn, are amplified as they convect downstream and can eventually trigger a new merging. Upstream acoustical propagation with velocity $a - \bar{U}$ will require transit times $\sim 3.6\tau$ (Run I) and $\sim 5.4\tau$ (Run Ix) for a disturbance generated at the downstream boundary to affect the shear layer near the inflow. Thus, by design, upstream effects associated with the first vortex pairing exiting the domain are not expected for $t \lesssim 10.6\tau$ for Run I and for $t \lesssim 15.4\tau$ for Run Ix.

These expectations are confirmed in Fig. 6. The flow features of Runs I and Ix depicted by this figure are virtually the same for $t = 6\tau$ and $t = 9\tau$ (top two rows), and for later times the simulated shear flow on the extended domain (on

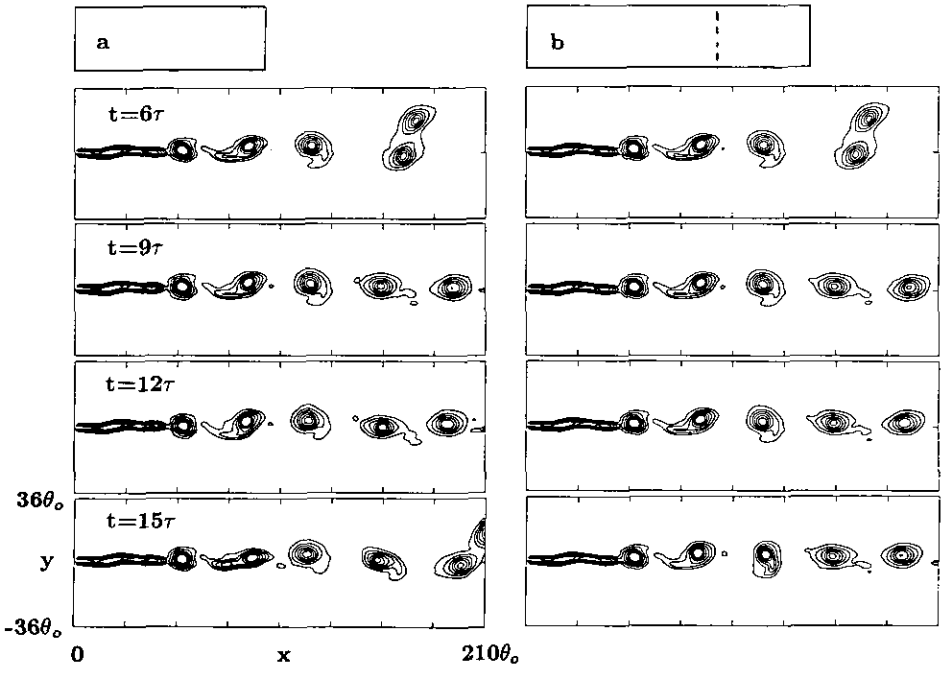

FIG. 6. Development of the forced mixing layer in nested computational domains in terms of vorticity contours: (a) Run I, simulation in the domain of Fig. 4; (b) Run Ix, simulation in a domain extending 50% farther downstream (flow outside smaller domain not shown). The scaled-down domains are indicated schematically on the top. Left and right boundaries of all frames correspond to the inflow/outflow boundaries in Fig. 4.

the right column) shows the downstream convection of vortices that are essentially undisturbed in the cross-stream direction. On the other hand, the shear layer in Run I on the left shows transverse modulation on the lower two rows. The timing of the modulation advancement in the streamwise direction can be explained in terms of upstream acoustical transit time required for a subharmonic disturbance generated at the downstream boundary at $t \approx 7\tau$ plus downstream convection time with velocity $\bar{U}$. These characteristic times can be used to explain the modulation advancement through roughly 65% of the domain by $t = 12\tau$, and then nearly throughout the whole domain by $t = 15\tau$, when it is leading to a new vortex pairing depicted near the downstream boundary. Figure 6 can also be used to isolate upstream feedback effects directly associated with acoustical disturbances generated by the first vortex pairing (present in both simulations) from those related to disturbances generated as the system of pairing vortices exits the computational domain (effectively present only for Run I). For the particular (relatively short) domains and (forced-flow) configurations considered here, the BC-*independent* effects turn out to be weaker.

Figures 7–8 focus on the developed flow at much later times—about 30 forcing periods later than the latest time in Fig. 5—and are used to further examine upstream effects of the outflow IOBC on the computational domain of Fig. 4, as a function of the parameter σ in (29). Figure 7 compares Run I using the one-dimensional non-reflective outflow IOBC provided by (30) (Fig. 7a), with Run II (Fig. 7b). Based on a one-dimensional picture in which (30) is a *perfectly* non-reflecting condition, using (29) with small non-vanishing σ can be regarded as having greater reflectivity, i.e., as allowing more incoming information—"natural reflections"— at the outflow boundary than in the case for $\sigma = 0$. A distinctive feature of the developed flow is the self-sustained occurrence of vortex mergings, this being a consequence of the feedback mechanism discussed above, by which the initial shear layer is disturbed by subharmonic perturbations generated downstream. These basic features are observed in both Figs. 7a and 7b. However, although Runs I and II exhibit similar features, the phase-reference of the events is clearly different; i.e., they occur at different times and space locations. These differences reflect the perturbation of the initial shear layer due to additional incoming acoustical waves that are allowed through the outflow boundary in Run II by having a non-zero σ in (30). As more of such incoming information is allowed—following, again, the one-dimensional picture—by further increasing the value of σ (Run III, Fig. 8), longer wavelengths are more appreciably excited through feedback in the initial shear layer. As a consequence, mergings involving previously merged vortices are now also observed and the mixing layer growth is faster.

Because there are no ideally defined downstream IOBC for free shear-flows, specifying $\mathscr{L}_1$—and the actual location of the outflow boundary—amounts to *defining* particular shear-flows studied. Thus, in the absence of additional externally given requirements (e.g., specific outflow IOBC from a laboratory experiment to be simulated, or specific expected near-field features to be emulated), even in a relatively simplified IOBC/CNBC framework such as discussed in this paper, $\mathscr{L}_1^{\text{exact}}$ and σ in (29) cannot be uniquely prescribed and the quality of the different shear flows specified by condition (29) can be compared only on subjective grounds.

The significance of the upstream feedback effects

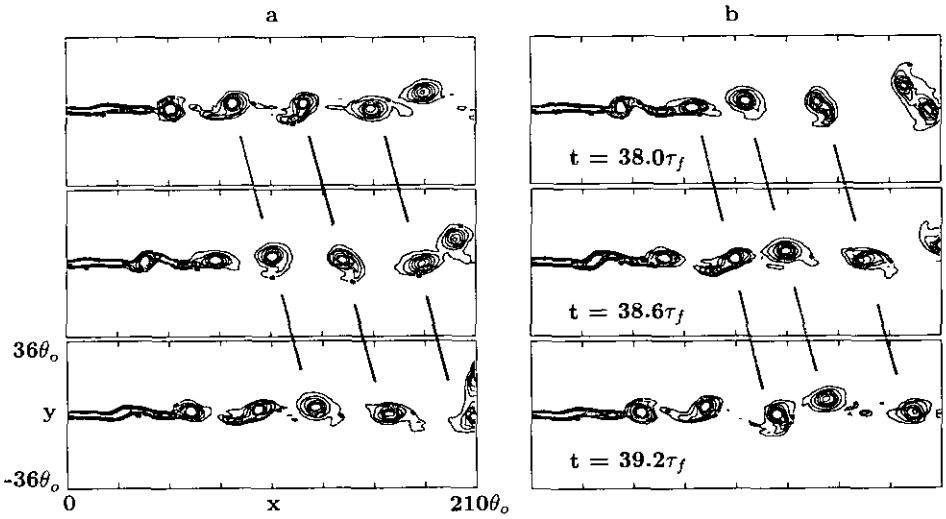

FIG. 7. Flow visualization of the developed forced mixing layer in the domain of Fig. 4 in terms of vorticity contours. Equation (29) with $\mathscr{L}_1^{exact} = 0$, $M = 0.57$, and $L = 130\theta_o$, is used as outflow IOBC: (a) Run I ($\sigma = 0$); (b) Run II ($\sigma = 2.7$). Left and right boundaries of the frames correspond to the actual inflow/outflow boundaries in the computational domain.

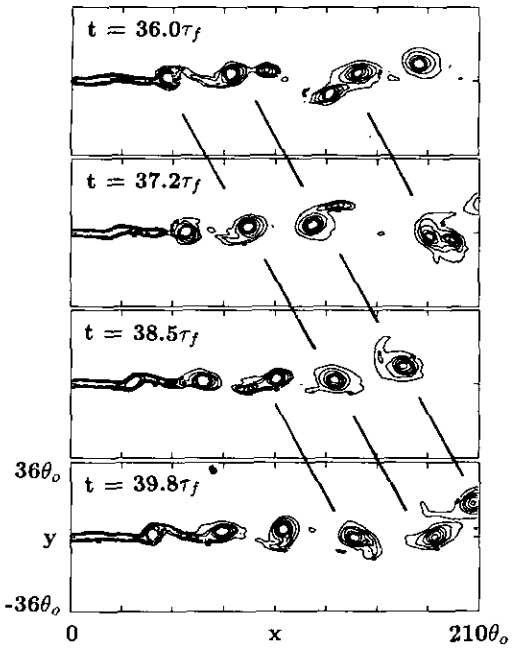

FIG. 8. Caption as in Fig. 6 for Run III ($\sigma = 10.8$).

associated with the outflow boundary conditions is likely to be reduced by choosing the outflow boundary farther away downstream or by increasing the forcing level at the inflow. However, these effects cannot be fully eliminated and they are particularly important in the case of unforced free shear-flows.

5. FINAL REMARKS

We have addressed basic difficulties associated with the specification of IOBC and CNBC for subsonic, unsteady free shear-flows. The discussion has included the limitations of simplified, time-independent open boundary conditions and the practical implementation of improved approaches based on one-dimensional characteristic analysis. An improved control of reflections at the downstream boundary in spatially developing shear-flow simulations will demand more general multidimensional approaches and BC analysis. Some of these approaches appear to be available in the mathematics literature but their actual transition to practical useful tools in turbulent shear-flow simulations remains to be investigated.

A crucial issue raised in this work is that of imposing appropriate outflow IOBC for specific shear-flow studies. The examples have illustrated the potential sensitivity of subsonic free shear-flows to the actual choice of outflow IOBC, which is an intrinsic feature of the flows being studied. In order to improve the characterization of these flows, through the combined efforts of laboratory and numerical experiments, it is essential to have information on the (generally not reported) far-field flow conditions imposed by the laboratory facilities, or at least, evidence of the extent of dependence of the experimental observations on IOBC and other BC besides the initial (inflow) boundary conditions.

APPENDIX

For the sake of the discussion in this paper, a convenient set of a LODI system of equations in the x_1-direction for the mass density, static pressure, momenta, and x_1-velocity, in terms of the $\mathscr{L}_i$, is the following:

$$\frac{\partial \rho}{\partial t} + \frac{1}{a^2}\left[\mathscr{L}_2 + \frac{1}{2}(\mathscr{L}_5 + \mathscr{L}_1)\right] = 0, \tag{A.1}$$

$$\frac{\partial P}{\partial t} + \frac{1}{2}(\mathscr{L}_5 + \mathscr{L}_1) = 0, \tag{A.2}$$

$$\frac{\partial u_1}{\partial t} + \frac{1}{2\rho a}(\mathscr{L}_5 - \mathscr{L}_1) = 0, \tag{A.3}$$

$$\frac{\partial \rho u_1}{\partial t} + \frac{1}{a}\left[M\mathscr{L}_2 + \frac{1}{2}\{(M-1)\,\mathscr{L}_1 + (M+1)\,\mathscr{L}_5\}\right] = 0, \tag{A.4}$$

$$\frac{\partial \rho u_2}{\partial t} + \frac{u_2}{a^2}\left[\mathscr{L}_2 + \frac{1}{2}(\mathscr{L}_5 + \mathscr{L}_1)\right] + \rho\mathscr{L}_3 = 0, \tag{A.5}$$

$$\frac{\partial \rho u_3}{\partial t} + \frac{u_3}{a^2}\left[\mathscr{L}_2 + \frac{1}{2}(\mathscr{L}_5 + \mathscr{L}_1)\right] + \rho\mathscr{L}_4 = 0. \tag{A.6}$$

Depending on the choice of flow variables, other sets of LODI equations are possible [20].

ACKNOWLEDGMENTS

This work was supported by the Office of Naval Research and the Naval Research Laboratory. The calculations were performed at the computer facilities of NAS at NASA Ames Research Center. The author acknowledges helpful discussions with W. K. George, G. Patnaik, J. P. Boris, K. Kailasanath, and R. Guirguis. He also thanks J. P. Boris and K. Kailasanath for their critical readings of the manuscript.

REFERENCES

1. C. M. Ho and P. Huerre, *Annu. Rev. Fluid Mech.* **16**, 365 (1984).
2. R. W. Metcalfe, S. A. Orszag, M. E. Brachet, S. Menon, and J. J. Riley, *J. Fluid Mech.* **184**, 207 (1987).
3. P. E. Dimotakis, *AIAA J.* **24**, 1791 (1986).
4. F. F. Grinstein, E. S. Oran, and J. P. Boris, *Phys. Fluids A* **3**, 2401 (1991).

5. J. C. Strikwerda, *Commun. Pure Appl. Math.* **30**, 797 (1977).
6. J. Oliger and A. Sundstrom, *SIAM J. Appl. Math.* **35**, 419 (1978).
7. R. W. Davis and E. F. Moore, *Phys. Fluids* **28**, 1626 (1985).
8. F. F. Grinstein, F. Haussain, and E. S. Oran, *Europ. J. Mech. B/Fluids* **9**, 499 (1990).
9. P. Givi and W. H. Jou, in *22nd Symposium (International) on Combustion*, pp. 635–643 (The Combustion Institute, Pittsburg, 1988).
10. G. Em. Karniadakis and G. S. Triantafyllou, *J. Fluid Mech.* **199**, 441 (1989).
11. K. Hannemann and H. Oertel, Jr., *J. Fluid Mech.* **199**, 55 (1989).
12. J. C. Buell and P. Huerre, Report CTR-S88, p. 19–28, Stanford, 1988 (unpublished).
13. D. Givoli, *J. Comput. Phys.* **94**, 1 (1991).
14. K. Thompson, *J. Comput. Phys.* **68**, 1 (1987).
15. T. Hagstrom and S. I. Hariharan, *Math. Comput.* **51**, 581 (1988).
16. E. Gutmark and C. M. Ho, *Phys. Fluids* **26**, 2932 (1983).
17. W. K. George, *Exp. Thermal Fluid Sci.* **3**, 557 (1990).
18. W. K. George, in *Advances in Turbulence*, edited by W. K. George and R. Arndt (Hemisphere, New York, 1989), p. 39.
19. B. Gustafsson, *Math. Comput.* **29**, 396 (1975).
20. K. Thompson, *J. Comput. Phys.* **89**, 439 (1990).
21. T. J. Poinsot and S. K. Lele, *J. Comput. Phys.* **101**, 104 (1992).
22. D. H. Rudy and J. C. Strikwerda, *J. Comput. Phys.* **36**, 55 (1980).
23. J. P. Boris, and D. L. Book, in *Methods in Computational Physics*, Vol. 16 (Academic Press, New York, 1976), p. 85.
24. B. Engquist and A. Majda, *Math. Comput.* **31**, 629 (1977).
25. F. F. Grinstein, R. H. Guirguis, J. P. Dahlburg, and E. S. Oran, in *11th Int. Conf. Numer. Methods Fluids Dynamics* edited by D. L. Dwoyer, M. Y. Hussaini, and M. Y. Hussaini (Springer Verlag, New York, 1989), p. 283.